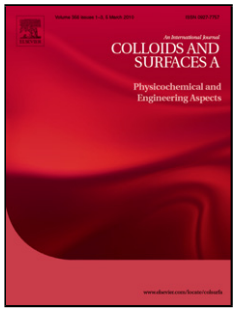

Title: Stability of stearic acid monolayers on artificial sea water

Authors: A.M. Brzozowska, M.H.G. Duits, F. Mugele

PII: S0927-7757(12)00321-4
DOI: doi:10.1016/j.colsurfa.2012.04.055
Reference: COLSUA 17660

To appear in: *Colloids and Surfaces A: Physicochem. Eng. Aspects*

Received date: 5-3-2012
Revised date: 23-4-2012
Accepted date: 24-4-2012

Please cite this article as: A.M. Brzozowska, M.H.G. Duits, F. Mugele, Stability of stearic acid monolayers on artificial sea water, *Colloids and Surfaces A: Physicochemical and Engineering Aspects* (2010), doi:10.1016/j.colsurfa.2012.04.055

Stability of stearic acid monolayers on artificial sea water

A.M. Brzozowska#, M.H.G. Duits*, F. Mugele

Physics of Complex Fluids group and MESA+ Institute, Faculty of Science and Technology, University of Twente PO Box 217, 7500 AE Enschede, the Netherlands,

** Corresponding author, e-mail: m.h.g.duits@utwente.nl.*

 # Present address: Institute of Materials Research and Engineering, 3 Research Link, 117602 Singapore

Abstract

We studied the formation and stability of Stearic Acid (SA) based films on aqueous sub-phases via Langmuir trough and imaging ellipsometry experiments. The aqueous phase was based on Artificial Sea Water (ASW), a multicomponent salt solution with a total molarity of 0.53. The composition of this solution was varied via dilution (1, 10 and 100 times) and adjustment of the pH (3, 7, 10). Also water sub-phases without the ASW salts were studied. Pressure-area isotherms of the SA monolayers show an enhanced stability of the film against fracture when the pH and/or the salt concentration of the sub-phase are increased. Isobars of SA measured below the pressure needed for film fracture, indicate distinct mechanisms for loss of material: 1) at low pH and salt concentration, three dimensional (3D) structures are formed at the air/water interface via nucleation and growth, and 2) at high pH and salt concentration, diffusion-controlled dissolution of molecules in the sub-phase occurs. The formation of multilayer structures was corroborated with ellipsometry images of the films after Langmuir-Blodgett transfer.

***Keywords**: Stearic Acid, monolayer stability, Artificial Sea Water, Langmuir trough, imaging ellipsometry*

1. Introduction

Interfacial layers of fatty acids (and derivatives thereof) are ubiquitous. In nature they can be found for example in the membranes of biological cells or in (oil and water containing) rock reservoirs. In industry fatty acid (derivatives) are used in food products and detergents, exploiting their spontaneous assembly at oil/water (O/W) and air/water (A/W) interfaces. The geometry of thus formed layers may be flat, like for macroscopic menisci, or curved, as with capsules or emulsions.

In many cases, the mechanical properties of the layer are of key importance to their functionality [1, 2]. For example, membranes of cells need to be deformable in various processes, thereby resisting shear and bending forces. When vesicles or emulsion droplets are subjected to flow, the interfacial layer coats have to accommodate bending, stretching or compression forces. In food or pharmaceutical products, the involved deformations should remain small enough to prevent droplet coalescence [3, 4]. However, also undesirable mechanical stabilisation can occur, like in enhanced oil recovery (EOR). Here layers of naphthenic acids and/or asphaltenes can stabilize O/W interfaces, and impair the separation of oil and water [5-7].

Understanding these mechanical behaviors, requires insight into the assembly and interactions of the amphiphiles at the molecular length scale [1, 8, 9]. Given the interfacial area per molecule and the compositions of the monolayer and fluid phases, the interfacial molecules will tend to assemble into a structure (or phase) that minimizes the free energy. The mechanical properties of the layer then follow

from the increase in free energy associated with the deformation. Defining the stability of an interfacial monolayer as the ability to withstand increasing surface pressure without losing its character of a two-dimensional equilibrium phase, different mechanisms for loss of stability can be distinguished. The largest surface pressure that an interfacial monolayer can sustain is the so-called fracture pressure π_f. Fracture [10] will occur if during an on-going compression, the interfacial molecules are unable to leave the monolayer, either because this is thermodynamically disfavored or because the compression is too fast [11]. A mechanical instability then results, in which the layer breaks up. The formed fragments may or may not merge upon further compression of the layer [12, 13].

Besides monolayer fracture, also a thermodynamically driven expulsion of the interfacial molecules can take place. Examples hereof are the formation of a 3D solid phase [13], [14] or the (compression-induced) dissolution of interfacial species into the sub-phase [13, 15, 16]. The occurrence of these processes makes the resistance of the layer against loss of its constituents an important aspect of its mechanical stability. The mechanism in which 3D crystals nucleate and grow in a direction perpendicular to the interface [17] has been proposed by Xu *et al* [18] and Carry and Rideal [19], demonstrated by Lee and Liu [13] and modeled by Vollhardt *et al.* [20]. Nucleation can only occur if the surface pressure exceeds the equilibrium spreading pressure (ESP) [14, 18]. Similar to the situation in bulk liquids, it involves an activation energy which diminishes upon increasing the surface pressure [21]. Alternatively, molecules may also get expelled from the monolayer by dissolution into the aqueous sub-phase (driven by a difference in the chemical potential). This mechanism has been reported by Patil *et al* [15, 22, 23] and Matuura *et al* [23], and modeled, amongst others, by Ter Minassian [24, 25]. The loss rate of the interfacial molecules depends on the curvature of the layer, the concentration (profile) in the sub-phase and the diffusion coefficient.

The occurrence of these scenario's (whether it occurs in an aqueous drop or in a Langmuir film) can strongly depend on the composition of the sub-phase. For interfacial layers of SA (pKa ≈ 10 [26-28]) on either O/W or A/W interfaces, acid dissociation plays a key role, since the stearate anion is much more interfacially active than the undissociated species [29, 30]. While increasing the pH provides the most direct way to enhance the dissociation, also the presence of salt can facilitate the deprotonation of the COOH group of SA [27, 31, 32]. Besides that, salt can also provide specific cations that can induce complexation of SA anions.

While the interfacial behavior of SA on aqueous sub-phases has been well-studied for simple or binary salt solutions [13, 33-41] the regime of highly concentrated multiple salt mixtures has hardly been addressed. These conditions are of importance in several practical situations. Several biological fluids (e.g. blood, bile, gastric or pancreatic juices [42, 43]) contain mixtures of electrolytes, at a total molarity of ≈ 0.1 M. Another example is the enhanced oil recovery processes, where often saline (sea) water of high molarity (≈ 0.5 M) is used to displace oil in the rock reservoir. Interestingly, recent findings indicate that significantly better recovery results are sometimes obtained with water of lower salinity [44]. These observations make it interesting to examine the effect of (multiple) salt concentration on the interfacial stability of thin films. In view of the importance of the dissociation of the fatty acid, also the pH of the aqueous sub-phase should be taken into account. Considering the complexity of this system (see Fig. 1), a systematic study of both variations is warranted.

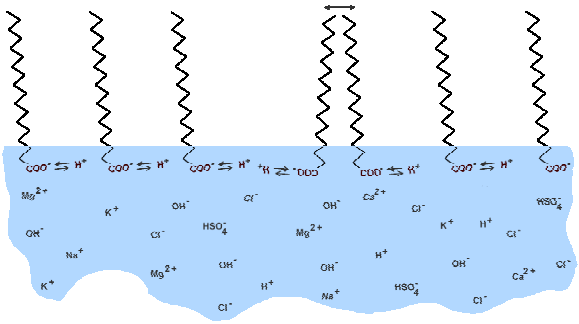

Figure 1. Schematic representation of possible interactions in a system with interfacial SA and various cations in the sub-phase. Interactions can be hydrophobic (between hydrocarbon chains) or electrostatic (between charged head-groups, or between charged head-groups and counter-ions)

In the present work, we explore a matrix of conditions, where the pH is set at 3, 7 and 10, and the salt concentration(s) at 0, 1, 10 and 100% times the concentration of so-called Artificial Sea Water (ASW) [45]. We investigate the effects of these aqueous sub-phase variations via Langmuir trough experiments (at the air/water interface). Here pressure vs. area (π-A) isotherms are studied for two purposes. First, to measure the characteristic surface pressures and molecular areas where transitions in the layer state (including fracture) occur. These quantities are very suitable for revealing the (sometimes subtle) effects of varying the pH and salt concentration. Secondly, the (π-A) isotherms are used as a reference for defining a constant surface pressure in follow-up experiments. These experiments entail both film relaxation experiments, aimed at detecting losses of interfacial material to another phase, and Langmuir-Blodgett transfers to enable imaging ellipsometry. The latter technique is used in particular for detection and quantification of (2D or 3D) structures formed at the interface.

2. Materials and methods

2.1. Chemicals and solutions

Octadecanoic acid (stearic acid, grade 1, approx. 99%, S4751-100G) was purchased from Sigma, and chloroform ($CHCl_3$, ACS reagent, 319988-2L) from Sigma-Aldrich. 0.1M standard solutions of NaOH (71395-1L) and HCl (49015-1L) were purchased from Fluka. Solutions of SA were prepared in $CHCl_3$ at concentrations of approximately 1 mg/ml. Artificial Sea Water (ASW) is a 10 component mixture with total concentration of approximately 0.53 M [45]. Specifically, it consists of: NaCl (426 mM, S7653-1KG), $NaSO_4$ (29.4 mM, 23859-7), KCl (9.45 mM, P3911-1KG), $NaHCO_3$ (2.43 mM, S6014-1KG), KBr, (0.86 mM, 24341-8), H_3BO_3 (0.44 mM, B0394-1KG), NaF (0.074 mM, 201154-500G), $MgCl_2{\times}6H_2O$ (55.5 mM, M9272-1KG), $CaCl_2{\times}2H_2O$ (10.8 mM, 22350-6) and $SrCl_2{\times}6H_2O$ (0.094 mM, 255521-500G). All these salts were of ACS reagent grade and were purchased from Sigma, and used as received. Dilutions of ASW were prepared with ultrapure water (18.2 MΩcm, Millipore Synergy UV system). The pH was adjusted with 0.1M NaOH or 0.1 M HCl. The change in concentration of Na^+, H^+, Cl^-, and OH^- due to pH adjustment was very small also as compared to 100 times diluted ASW.

2.2. Experimental techniques

Pressure-area (π-A) isotherms and (A-t) isobars were determined with an automated Langmuir trough (NIMA model 1212D1) equipped with a pressure sensor and a dipper. All measurements were carried out at room temperature (22.5 ± 0.5°C), which was monitored continuously together with the humidity. To reduce contamination with dust and to ensure stable measurement conditions, the trough was placed on a floating table and surrounded by a home-built laminar flow box. The airflow in the box was stopped during measurements. Prior to experiments the trough was rigorously cleaned with pure water and chloroform. After filling the trough with freshly prepared sub-phase, impurities were removed via suction of the top layer (using a NeoLab GmbH vacuum system). The interface was considered clean if the pressure change during consecutive compression and decompression of the interface was less than 0.1 mN/m. SA solutions in chloroform were spread at the interface (initial surface area S= 500 cm^2, corresponding to 0.40 nm^2/molecule) with a 50 µL Hamilton micro-syringe. After spreading, the film was allowed to equilibrate for 30 min. In subsequent measurements, films were compressed at constant rate dS/dt of 10 cm^2/min, and π was measured continuously using a Wilhelmy plate (filter paper) attached to a force sensor. Given the trough area S, the area A per molecule was calculated assuming that no molecules had left the interface.

For each sub-phase composition, at least five π-A isotherms were measured to ensure the reproducibility. The isotherms, of which the encountered shapes (along with some definitions) are shown in Fig. 2, were also used as a reference for defining the surface pressure in film relaxation measurements. In these isobaric experiments, which were typically performed twice per (pH, c_{ASW}) condition, the monolayer was compressed to a target pressure π, which was subsequently maintained by automatic adjustment of the film area. Isobars of the most stable films were recorded up to several hours.

Langmuir-Blodgett transfers were performed to allow studying the morphology of the interfacial layers *ex-situ*. As a substrate, we used CZ silicon wafers (Type P, boron doped, 100 from Okmetic) that had been cleaned, thermally oxidized and diced into 1×5 cm^2 pieces under clean room conditions. Films were transferred at a speed of 2 mm/min and at a surface pressure of 30 mN/m. The choice for this low speed was made to allow for complete water drainage and preservation of the structure of the floating film. The selected surface pressure of 30 mN/m should ensure that the layer was in the γ-regime during the transfer. The morphology of the transferred films was analyzed within 24 hours after the transfer, using an imaging ellipsometer at a wavelength of 658 nm (EP3 Nanoscope, Accurion). With this technique, absolute thickness maps of the material are obtained in a non-invasive manner, by measuring the ellipsometric angles ψ and Δ for each location ('pixel' size: 1.07 x 1.07 $µm^2$) on the substrate, and using the (complex) refractive indices n_i of both layer and substrate along with the Fresnel equations to translate (ψ, Δ) into a thickness d_i [46, 47]. Fitting ψ and Δ for the bare substrate with a two-layer model (Si: $d \rightarrow \infty$,n= 3.96 – 0.02i and SiO_2: n=1.46) yielded a typical d_{SiO2} of 40 nm, (precision per wafer 0.1 nm, variation between wafers 2 nm). The thickness of the transferred SA layers was calculated using a three-layer model, assuming a refractive index of 1.43.

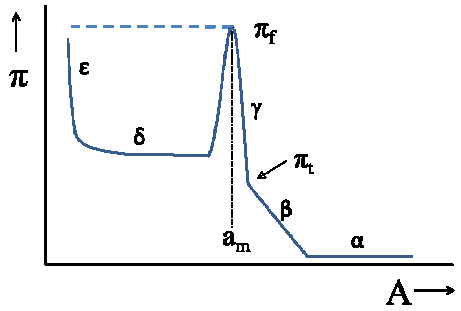

Figure 2. Schematic representation of encountered surface-pressure vs. area per molecule (π–A) isotherms. The maximum packing density corresponds to a molecular area of a_m. Upon compression of the interfacial molecules, the film undergoes transitions from a low density α-state via a β-state, to a high density γ-state. The transition from β to γ is marked with π_t. Beyond the point of the film fracture at π_f, π may either remain constant (constant pressure collapse, dashed line) or show a rapid decrease, a stabilization (δ) and a subsequent increase again (ε) (constant area collapse, solid line). For SA monolayers on (almost pure) water sub-phases, the precise nature of the states have been identified, and a nomenclature exists (e.g. [48-50]).

3. Results and discussion

3.1. Pressure-area isotherms of SA

The pressure-area isotherms given in Fig. 3 show remarkable changes, both upon variation of the pH and upon increasing the salt concentration c_{ASW} from 0 to 100%. We first discuss the most significant trends and features.

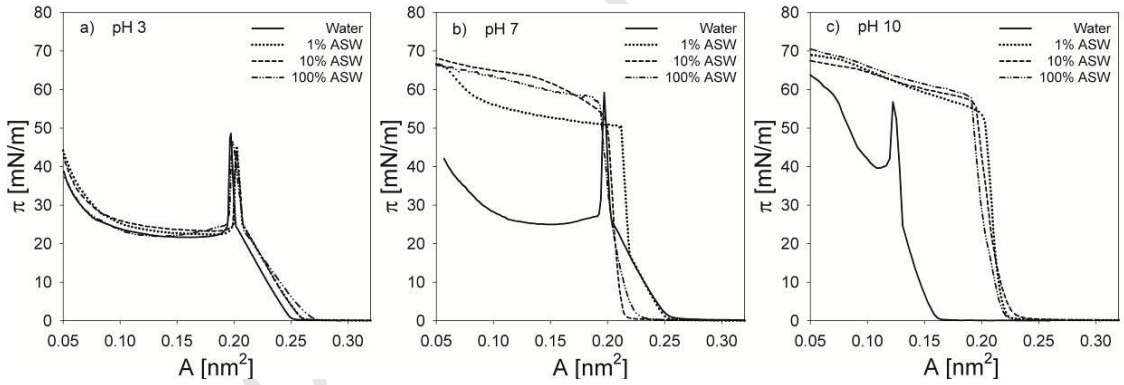

Figure 3. π – A isotherms of stearic acid films on Artificial Sea Water sub-phase of varying total salt concentration and pH. A – area per molecule, π – change of the interfacial pressure upon film compression. The concentration of Na^+ ions in pure water sub-phase due to pH adjustment is 0.09 mM and 1 mM for pH 7 and 10, respectively.

3.1.1. Dependence of isotherms on pH and c_{ASW}

Several global trends are observed upon variation of the pH. The signatures of the isotherms are very different at pH 3 (Fig. 3a) and pH 10 (Fig. 3c). Whereas at pH 3 a 'constant area collapse' is found, at pH 10 most isotherms show behavior resembling a 'constant pressure collapse'. Another difference is that at pH 10 the fracture pressures π_f are significantly larger than at pH 3. In contrast, the surface pressures π_t are much lower at pH 10. The molecular area A where the first non-zero π is encountered (upon compression) is also smaller at pH 10.

Several features in the isotherms at pH 7 can be viewed as a transition between the signatures at pH 3 and pH 10: in Fig. 3b both 'constant area' and 'constant pressure' collapses are encountered, and likewise for the occurrence of either a broad or a narrow β-regime (in the sense of the A-range). The isotherms at pH 7 appear to be very sensitive to the salt concentration, at least for $c_{ASW} \leq 10\%$.

Due to the strong differences between the π-A isotherms at pH 3 and pH 10, it is questionable whether one should speak of a global (i.e. pH independent) effect of varying the c_{ASW}. One feature which is common to all pH's, is that a 'constant area collapse' signature is observed at c_{ASW}=0. A salient detail here is that the (apparent) molecular area where this occurs at pH 10 (0.13 nm^2/molecule), is much lower than usual. For $c_{ASW} > 0$ the effects of increasing the salt concentration are clearly pH dependent. At pH 3 the β-regime (and to a lesser extent also the γ-regime) becomes more expanded, whereas at pH 10 it is hard to point out a clear trend, apart from the abrupt change that takes place at $0 < c_{ASW} < 1\%$. At pH 7, an intriguing transition is found around $c_{ASW} \approx 1\%$: while the β-state resembles the one at $c_{ASW} = 0$, the transition to the γ-state occurs at an area per molecule that is clearly larger than for all other c_{ASW}. This observation was well reproducible.

3.1.2. Mechanistic aspects

In this section we give tentative explanations for the observed isotherms. The isotherms at pH 3 should correspond to the presence of uncharged SA molecules at the interface. This expectation, based on the high pKa ≈ 10 as found for SA in assembled states [27, 28], is confirmed by our experimental observations: i) all isotherms at pH 3 have a 'constant area collapse' signature, regardless of the salt concentration. This signature, associated with fracture into multilayer structures that coexist with bare interface, has been found also in other cases where the interface was essentially uncharged [35]. ii) the effect of varying c_{ASW} on other characteristics of the isotherm is modest, as compared to the other pH values. The picture of uncharged SA at low pH has also been suggested in previous studies on SA monolayers, on sub-phases of simple or binary salt solutions [27, 34, 35].

At pH 7 presumably a small fraction of the SA molecules is charged. Adding ASW salt appears to have multiple effects, which become manifest in different ranges of c_{ASW}. At c_{ASW}=0 the dissociation of SA seems to be marginal, as suggested by the similarity to the isotherm at pH 3. For all $c_{ASW} > 0$ the interface is occupied with significant amounts of dissociated SA species at pH 7. This is suggested by the disappearance of the constant-area collapse signature [35].

Increasing c_{ASW} to 1% ASW appears to increase the acid dissociation, thereby causing electrostatic repulsions between the SA anions. At intermediate intermolecular distances (0.28 down to 0.23 nm^2/molecule) these forces appear to be weak, but at smaller distances they become significant, causing appearance of the γ-regime at a relatively large value of A (0.22 nm^2/molecule). It is here remarked that in a bulk solution with c_{ASW}=1%, the Debye length κ^{-1} [51] amounts a few nm, which is of the same order or magnitude as the intermolecular distance in the β-state. This κ^{-1} is reduced 10-fold on increasing c_{ASW} to 100%.

For c_{ASW} >> 1% the salt-induced SA dissociation still occurs, but an additional mechanism comes into play, making the β-regime almost disappear and reducing the minimum intermolecular distance back to its expected value; i.e. a_m = 0.20 nm^2/molecule. This might be attributed to the formation of cation

bridges between adjacent SA anions. This process is enhanced in particular by the binding of divalent cations such as Ca^{2+} or Mg^{2+} [52]. Such cation bridges could cause electrostatic attractions at intermediate distances between ionized SA species [53] whereas at shorter distances they might enforce a higher packing density of the aliphatic chains [36].

At pH 10, *i.e.* very close to the pK_a, a substantial fraction of the SA molecules should be charged, at all salt concentrations. For $c_{ASW} \geq 1\%$ the isotherms have the same signature as for $c_{ASW} \geq 10\%$ at pH 7, suggesting that both the enhanced SA dissociation and the ion bridging effects occur. The finding that this occurs at lower c_{ASW} at pH 10 is in line with the picture that enhancements of pH and ASW salt concentration work together in making a larger proportion of SA species available for cation complexation at the interface. The remarkable difference between the shapes of the isotherms at c_{ASW}=0 (with 1 mM monovalent ions present) and for $c_{ASW} \geq 1\%$ could be due to the divalent cations in the ASW.

The occurrence of a 'constant area' collapse at an unphysically low a_m of 0.13 nm^2/molecule suggests that at pH 10 and c_{ASW}=0, dissociated SA species get removed from the interface. Further evidence for this was obtained from additional experiments, in which a sequence of cleaning the interface, spreading SA and measuring the isotherm was repeated without replacing the sub-phase. Here it was found that the value of a_m progressively increased with each experiment. This clearly shows that SA can dissolve in the sub-phase (presumably as sodium stearate), and that the dissolution from the monolayer slows down as the sub-phase concentration gets higher. We observed this effect only on the sub-phase at 0% ASW and pH 10.

3.2. Morphology of SA films

LB transfers were done at π=30 mN/m, corresponding to the γ-regime of the monolayers. Representative film-thickness maps determined with ellipsometry and typical cross-sections thereof are shown in Fig. 4. Here it is remarked that even with the large sample-areas that were probed (350 µm x 350 µm), the total amount of material showed slight variations with the chosen (X, Y) region of interest. Another noteworthy aspect is that the time needed for a single LB transfer, was approximately 15-20 minutes. This means that ongoing changes in the layer structure during transfer (like 3D solid formation) cannot be excluded.

Considering all 12 thickness maps in conjunction with the isotherms in Fig. 3 (both were measured at the same subphase compositions), we observe a remarkable correlation: at the (pH,c_{ASW}) combinations where the isotherms show a 'constant area collapse', the LB layers show crystal-like structures, while at the (pH, c_{ASW}) combinations where the isotherms show a 'constant pressure collapse' the layers appear to be smooth. Quantitative details are discussed below.

Sub-phases without ASW

First we consider films formed on sub-phases with c_{ASW}=0. While the isotherms at pH 3 and 7 look very similar, inspection of the films with ellipsometry reveals remarkable differences in morphology. At pH 3 (where the ESP of SA on a water sub-phase ≈18 mN/m [14]) we observe sharp-edged, solid-like structures with large areas in between them. The typical lateral size of the structures is 50–100 µm, while their height ranges from 5 to 30 nm, indicating that they are multilayer assemblies (a stretched SA molecule is ~2.5 nm long [39]). The area between the aggregates turns out to be bare interface.

These observations clearly indicate the tendency of uncharged SA molecules to form 3D structures at the A/W interface at pH 3. It appears that at this low pH, the undissociated carboxylic head groups allow the hydrophobic interactions between the fatty-acid chains to dominate, and hence drive the aggregation.

At pH 7 (ESP ≈15 mN/m [13]) we observe solid aggregates with a very different morphology. Most of the sample area is covered with large structures that are built up from much smaller units. Their height is in the 15-20 nm range, indicating significant growth in the direction perpendicular to the interface. These aggregates coexist with areas of what appears to be bi- and mono-layers. These findings correspond well, and expand to the results of Lee and Liu, obtained with Brewster Angle Microscopy directly on the Langmuir trough [13]: their Fig. 8a-3, taken after a comparable waiting time, looks rather similar to a projection image (losing the height information) of our data.

At pH 10, where dissolution of SA into the subphase occurs (Sec. 3.1.2), a relatively homogeneous film is formed. Locally we still observe some sparse multilayer aggregates. These changes in morphology should probably be ascribed to enhanced electrostatic repulsions as compared to pH 7. These forces counteract the attractive chain-chain interactions and diminish the driving force for aggregation.

Effects of adding ASW salt

In the presence of salt (c_{ASW} ≥ 1%), the morphologies of the films change significantly. At pH 3, sharp-edged aggregates are still found but they become much thinner at 100% ASW. Also a coexistence of the fragments with areas of monolayer is found, suggesting a stabilizing effect of ASW on SA mono-layers. This is most prominent at c_{ASW} = 1% and becomes less significant at higher salt concentrations. A second observation is that for c_{ASW} 10 or 100%, bare areas are mostly found in the direct vicinity of the multilayer structures, suggesting growth of the latter at the expense of the former. The relative occurrence of bare and monolayer areas might indicate how far the nucleation and growth had progressed at the time of the LB transfer. It would then be suggested that the c_{ASW} dependence of the nucleation rate shows a local minimum at 1% ASW.

At pH 7 the addition of ASW salt causes a drastic change: instead of a large volume of aggregates, thin homogeneous films are formed. Their thickness corresponds, within experimental error, to a mono-layer. An exception is the film formed at 10% ASW, where thickness of 1 nm is found. This might be the result of an imperfect LB transfer, leading to SA chains that are tilted with respect to surface normal. Remarkably, the layer transferred from a sub-phase at 1% ASW does not show any special morphology, in spite of the deviatory isotherm (see Fig. 3b). Considering the overall effect of adding ASW salt, it is implied that electrostatic effects play a key role in the formation of homogeneous layers. This might involve both repulsive and attractive interactions, as discussed in Sec. 3.1.

At pH 10, predominantly smooth films are obtained in the presence of ASW. A drastic increase in film thickness is found upon increasing c_{ASW} from 0 to 1% ASW. On further increasing c_{ASW} the thickness becomes smaller again. The thicknesses found at 1 and 10% ASW are clearly above that of an SA monolayer. Since neither the isotherms (Sec. 3.1) nor the isobars (Sec 3.3) provide a clue about the microscopic origin of the formation of these thick layers, we can only speculate that it might involve folding [54] of several monolayers, or the entrapment of water underneath the (SA) film [55]. This would require further study, which is beyond the scope of this paper.

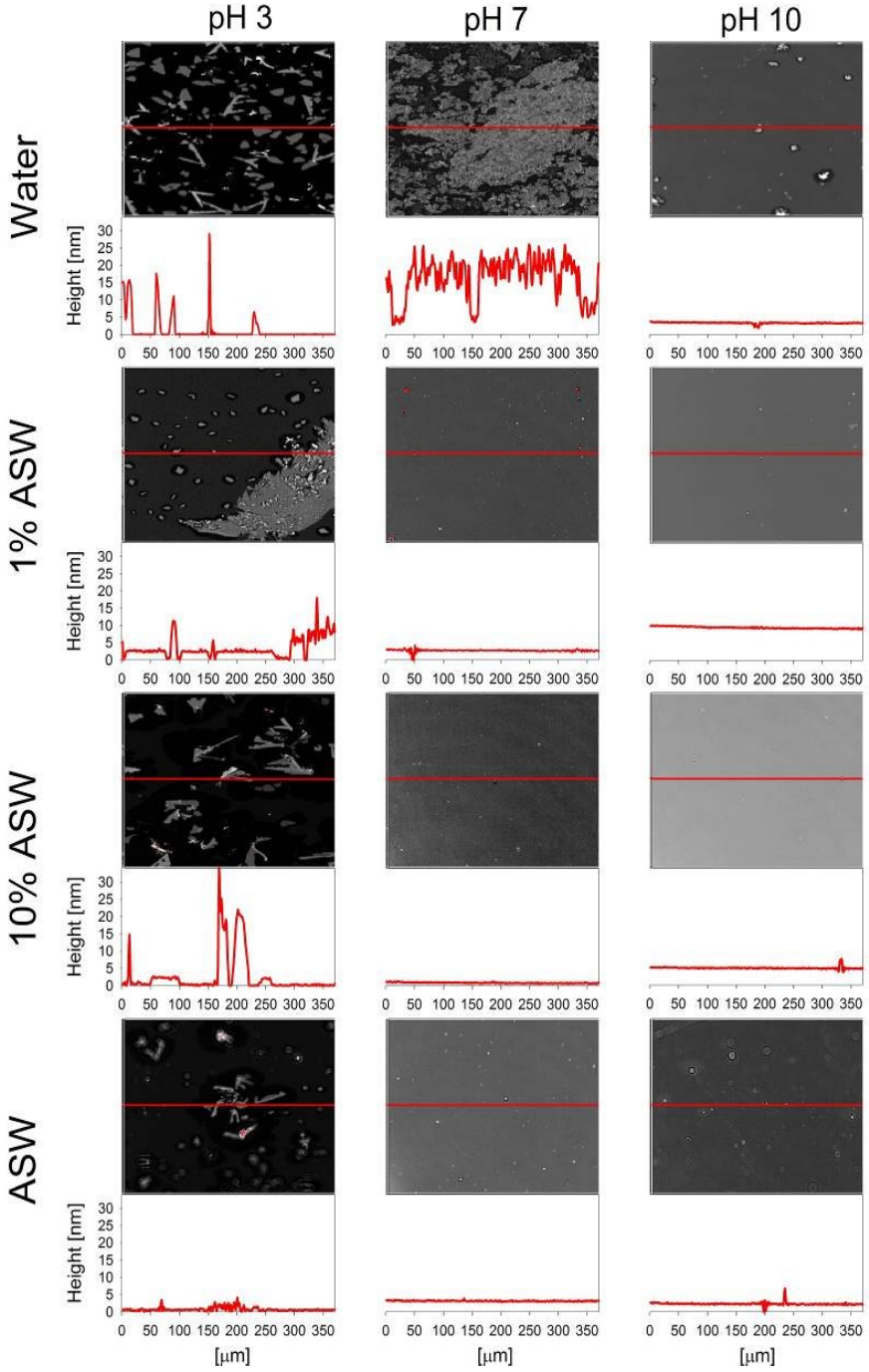

Figure 4 (color online). Thickness maps of SA films transferred onto silica substrates from air – liquid interfaces. Liquid sub-
315 *phase was ASW of varying total salt concentration and pH. Films were transferred at constant pressure of 30 mN/m. Below each map we show a thickness profile along the red line marked on the map. The y-axis scale is the same in all graphs.*

3.3. Relaxation of SA films

3.3.1. Isobars

To examine the mechanisms for loss of layer stability via the expulsion of material, we performed Langmuir trough experiments in which the surface pressure π was maintained at a constant level, and the change of the film area was measured as a function of time. Based on the measured isotherms (shown in Fig. 3), two π-values were studied per (pH, c_{ASW}) condition: one just below the fracture pressure π_f and one significantly lower, but still above the (estimated) Equilibrium Spreading Pressure. This should allow studying different modes of monolayer collapse, where we characterize collapse as an accelerating loss of monolayer area over time [19].

Figure 5 shows the film relaxation curves as A/A_0 vs. t, where A_0 is the area at the beginning of the relaxation experiment; any losses of interfacial SA that occur before reaching the target π (during equilibration) are thus 'normalized out'. The corresponding absolute areas A_0 can be looked up from Fig. 3, and indicate that (except for pH=10 and c_{ASW}=0) the loss of SA during the equilibration period was generally very modest. At pH 3, the relaxation behaviors are very different for the two surface pressures. At π = 20 mN/m, where SA film is still in the β-state, the changes of the film area in time are so minor that it is difficult to assess the effect of varying the salt concentration. However at π =30 mN/m where film is the γ-state, the film area shows a five-fold reduction in less than one hour. For all c_{ASW} an S-shaped relaxation is observed. The area decrease appears to become slower as c_{ASW} is increased. However the trend is not regular, considering the interchanged locations of the curves at 1 and 10% ASW.

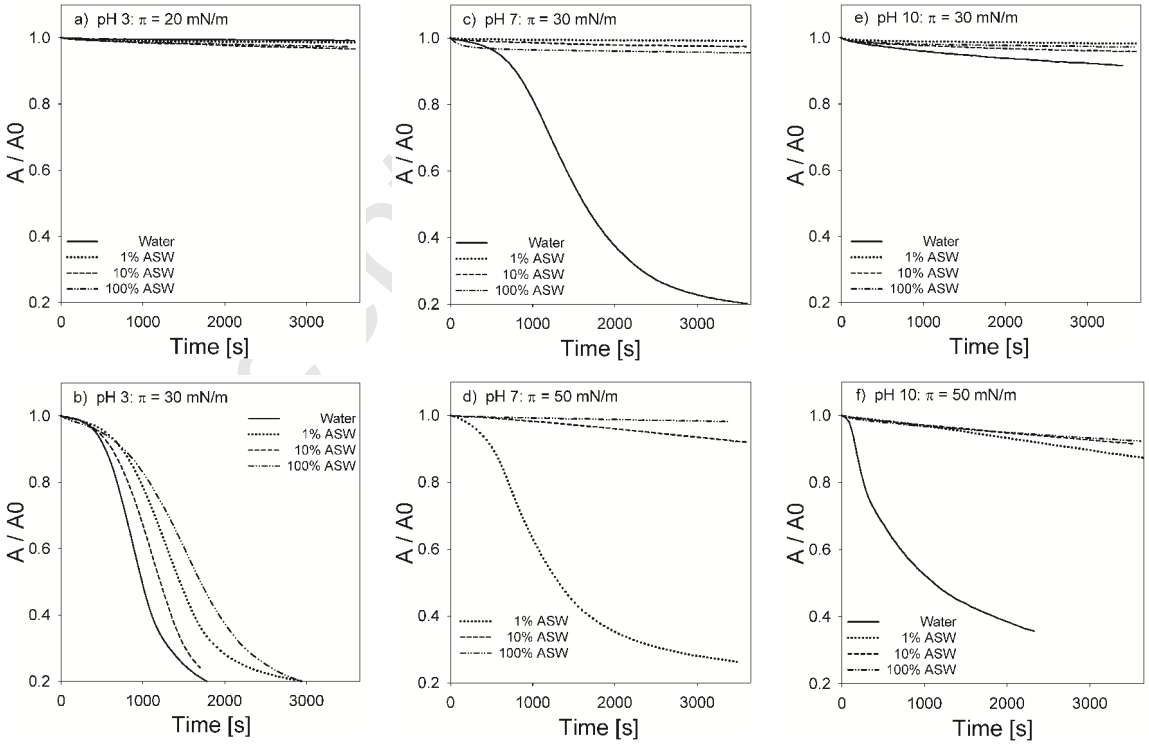

Figure 5. Relaxation curves of SA films determined on sub-phase of varying c_{ASW} and pH. Axis scaling is the same in all figures. Note that the ordinate starts at 0.2.

Combining these observations with our earlier findings at pH 3, it is clear that the loss of material at π =30 mN/m is due to the formation of a 3D solid phase. This explanation, which was also proposed by others [19], [40], [56] (albeit for sub-phases containing only single or binary salts) is supported by our observation of solid-like morphologies shown in Fig 4, that were found at the same pH and π. We did not find any kinked A(t) curves, indicative for trilayer formation [35].

When the pH is raised to 7 or 10, the film relaxations follow S-shaped A(t) curves only for some SA layers that were formed on 'low-salt' sub-phases (c_{ASW} = 0 or 1%). Analyzing the A(t) curves in conjunction with the isotherms and the ellipsometric thickness maps, it appears that several separate cases need to be distinguished. At pH 7 and 0% ASW the SA should hardly be dissociated [27], and therefore be able to form nuclei of 3D solid phase. This should explain the S-shaped curve at π =30 mN/m. We note that the initial part of this curve corresponds well to that in ref [13]. At pH 7 and 1% ASW the SA molecules probably dissociate without significantly binding to cations, resulting in charged interfacial assemblies that cannot form nuclei anymore, due to the strong electrostatic repulsions. A very high surface pressure (π =50 mN/m) needs to be imposed in order to observe expulsion of SA. Considering that the measured fracture pressure is only marginally higher for this sample, it cannot be excluded that the S-shaped curve is due to monolayer fracture.

At pH 10 the SA can partly dissolve into the sub-phase, at least at 0% ASW (see Sec. 3.1.2.). Also 3D solid phase formation can occur at this sub-phase condition (see Sec 3.2.). It is therefore conceivable that both mechanisms can contribute to the film relaxations at pH 10 (with each mechanism depending on c_{ASW} and π). At π=30 mN/m all loss rates dA/dt are rather small. The highest rate, observed at 0% ASW, is still much smaller than the average dA/dt during the equilibration time (in which dissolution took place). It might correspond to a late stage of the SA dissolution that was started upon spreading (π ≈ 0), but could also be due to an enhanced solubility at π=30 mN/m. Besides that, since 3D solid formation was observed under this condition (Fig. 4), also this could contribute to the measured dA/dt. In any case it is clear that adding ASW salts increases the stability of the film. At π=50 mN/m all loss-rates are higher. Again this could correspond to (pressure induced) dissolution of SA and/or nucleation and growth. This will be further explored in Sec. 3.3.1 where comparisons with models are made.

Looking at the entire dataset of Fig. 5, the principal trend is that a higher pH and/or a higher c_{ASW}, disfavor the occurrence of S-shaped relaxation curves, and the formation of 3D solid phase. This corroborates our earlier interpretation that (probably the divalent) cations in the salty water favor the formation of (thermodynamically more stable) metal-stearates at the interface; here the pH facilitates the deprotonation whereas the ASW provides the (divalent) cations for complexation [30].

3.3.1. Comparison to theoretical models

In this section we present a quantitative analysis of the relaxation curves in Fig. 5, by comparison to two theoretical models: i) formation of 3D solid phase at the A/W interface and ii) dissolution into the sub-phase. In different models by Vollhardt et al (see [21] for a recent overview) the formation of a 3D solid phase (at surface pressures above ESP) is described via nucleation [20, 57] and growth [14] processes. Other processes that remove molecules from the interface (like desorption) are supposed to be negligible, which in the case of SA on water sub-phases with low pH was proven to be justified

[21]. Taking into account several possible geometries for the nucleating structures, and considering the overlap of growing nuclei, the following general expression for A(t) was obtained:

$$\frac{A_0 - A(t)}{A_0 - A_\infty} = 1 - \exp(-K_x(t - t_i)^x) \qquad \text{(Eq. 1a)}$$

Here *A(t)* is the film area at time *t*, and the subscripts 0 and ∞ pertain to the corresponding limiting values of *t*. Fit parameters in the model are the nucleation constant K_x, the induction time t_i and the exponent *x*, which should reflect the geometry for nucleation (and subsequent growth). Specifically, *x*=1.5 or 2.5 for hemispheres and 2.0 or 3.0 for cylinders showing edge growth (under somewhat simplifying assumptions) [57]. All isobars that show an accelerated decrease of *A* over time were analyzed with Eq. 1. Instead of using the values of *x* corresponding to the various known mechanisms as input, and optimizing K_x and t_I to get the best fit to the linearized Eq. 1, we have performed a least-squares fit of our data with Eq. 1a, using not only K_x and t_i but also *x* as a (simultaneous) fit parameter. The proximity of the obtained *x* to the known cases should then give indications about the nucleation geometry and kinetics.

The results shown in Table A1 (Appendix) indicate that fairly good fits were obtained (correlation coefficient R^2>0.99) for t ≤ 1200 s. At longer times deviations from the model became significant. Remarkable variations are found in the exponent *x*. The most consistent picture is found at pH 3, where x ≈ 3 for all c_{ASW}, except 100% ASW where it is 2.2. The relaxation curves at pH 7 give x ≈ (3, 2.3) for c_{ASW}= (0,1%) respectively. These values appear to be roughly in agreement with the previously suggested nucleation and growth mechanisms, which indicates that 3D solid phase formation occurs for all ASW concentrations at pH 3. One fact that remains, is that our morphologies show sharp-edged (rather than rounded) structures. At pH 10, fitting the model to the experimental data yields x=0.7. This number is too low to be related to any of the described model cases, possibly suggesting that nucleation is not the dominant loss mechanism at this pH.

The model by Ter Minassian-Saraga [24, 25] considers the loss of interfacial material via ionization and subsequent diffusion of the molecules into the sub-phase. Assuming that the diffusion is rate-limiting, and that the medium is an infinite half-space, A(t) is described with:

$$\ln\left(\frac{A}{A_0}\right) = -2\frac{C_0}{\delta}\sqrt{\frac{D}{\pi}}\sqrt{t} \qquad \text{(Eq. 2)}$$

where A_0 is the initial area of the film, δ the density of the monolayer [mass/area], C_0 the concentration of the diffusive species adjacent to the monolayer [mass/volume], and *D* the diffusion coefficient. Patil *et al* [15] found that for fatty acid films, the desorption kinetics changes in time: initially $ln(A/A_0)$ shows a linear decrease with $t^{1/2}$, but in a later stage the scaling goes with *t*. The underlying picture is that in the initial stage a concentration profile has to be set up. The corresponding desorption coefficients are defined as:

$$K_1' = -\frac{d\ln(A/A_0)}{d\sqrt{t}} \quad \text{(Eq. 3a)} \quad \text{and} \quad K_2' = -\frac{d\ln(A/A_0)}{dt} \quad \text{(Eq. 3b)},$$

Most *A(t)* curves that showed a monotonous (but not S-shaped) decrease, were analyzed with dissolution model. An exception was made for a few curves, for which the decrease in A was too small to make a significant fit. Replotting the data from Fig. 5 as $ln(A/A_0)$ vs both $t^{1/2}$ and *t*, indeed a transition from the behavior of Eq. 3a to that of Eq. 3b was found (see Fig. A1 in Appendix). For all considered pH values a good agreement with the model was found for c_{ASW} ≥10%. The corresponding desorption coefficients K'_1 and K'_2 can be found in Table A2 (Appendix). The most significant trend in this table appears to be, that both desorption coefficients increase with pH. This indicates that the solubility of the interfacial layer increases with pH. At pH 10 where the solubility is highest, the addition of more ASW salt appears to lower the desorption rate. A similar stabilizing effect of the sub-phase ionic strength has been found earlier [58].

3.4. Overview

Finally we summarize the qualitative findings from the different experiments in Figure 6. It appears that in spite of the chemical complexity of the system, the correlation between phenomena and conditions (pH, c_{ASW}) is quite strong. This seems to suggest that the collective behaviors of the layers are largely determined by the properties (acid dissociation, ion binding) at the molecular level.

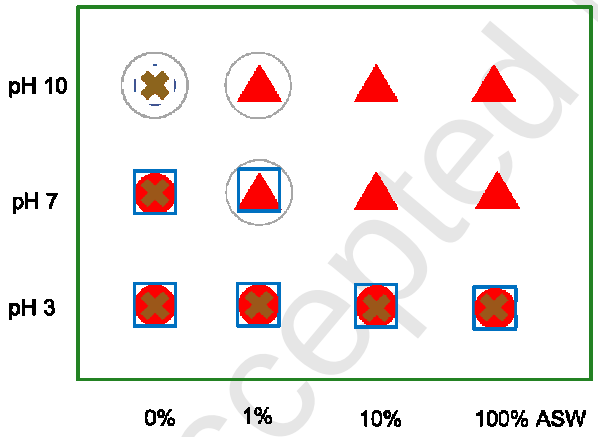

Figure 6 (color online). Overview of the behaviors of SA monolayers in different experiments, as a function of the pH and c_{ASW} of the aqueous sub-phase. ●/▲ and □ are obtained from the isotherms and indicate constant area / constant pressure collapse respectively the presence of a β-regime with a broad A-range (see Fig. 3). x denotes where 3D solid phases were observed in the morphology maps (Fig. 4). ○ indicates where dissolution of interfacial molecules into the sub-phase occurred (see Fig. 5). In cases where the effects were weak, the plot symbols have been given a higher transparency.

4. Conclusions and Outlook

Monolayers of stearic acid on aqueous sub-phases can lose stability via dissolution into the sub-phase, via 3D solid formation at the air/water interface and via fracture. The occurrence of these mechanisms, which is of relevance to various fields in science and technology (biology, food, oil recovery), was studied for several combinations of salt concentration and pH value, using sub-phases based on Artificial Sea Water. Formation of 3D solid phase occurs mainly under acidic conditions (pH 3) where the SA molecules are uncharged. Dissolution can occur under basic conditions (pH 10), where it can be suppressed by increasing the salt concentration. Fracture ultimately occurs upon continued compression of the interface. The required surface pressure generally increases with pH, while also the fracture mechanism changes, from a 'constant area' collapse at pH 3 to a predominantly 'constant pressure' collapse at pH 10. Increasing the salt concentration has strong effects at pH 7, where it suppresses formation of 3D solid phase, and at pH 10 where it suppresses dissolution.

While the global effects of pH and salt concentration can be mechanistically understood by considering acid dissociation, electrostatic effects and ion binding, also some yet unexplained observations were made; in particular the behavior at low (100x diluted) ASW salt concentration. Also some clues were obtained that specific cations play a role; this warrants further study.

Acknowledgments

We acknowledge Mariska van der Weide and Klaas Smit for technical support. MHGD thanks Lei Wang for discussions. This project was financially supported by BP.

References

1. Miller, R., et al., *Rheology of interfacial layers.* Colloid and Polymer Science, 2010. **288**(9): p. 937-950.

2. Dickinson, E., *Adsorbed protein layers at fluid interfaces: interactions, structure and surface rheology.* Colloids and Surfaces B-Biointerfaces, 1999. **15**(2): p. 161-176.

3. Dickinson, E., *interfacial interactions and the stability of oil-in-water emulsions.* Pure and Applied Chemistry, 1992. **64**(11): p. 1721-1724.

4. Friberg, S., P.O. Jansson, and E. Cederberg, *surfactant association structure and emulsion stability.* Journal of Colloid and Interface Science, 1976. **55**(3): p. 614-623.

5. Alvarez, G., et al., *Small-Angle Neutron Scattering Study of Crude Oil Emulsions: Structure of the Oil-Water Interfaces.* Langmuir, 2009. **25**(7): p. 3985-3990.

6. Alvarez, G., et al., *Heavy Oil-Water Interfacial Properties and Emulsion Stability: Influence of Dilution.* Energy & Fuels, 2009. **23**(1): p. 294-299.

7. Jones, T.J., E.L. Neustadter, and K.P. Whittingham, *water-in-crude oil emulsion stability and emulsion destabilization by chemical demulsifiers.* Journal of Canadian Petroleum Technology, 1978. **17**(2): p. 100-108.

8. Lee, M.H., et al., *Combined Passive and Active Microrheology Study of Protein-Layer Formation at an Air-Water Interface.* Langmuir, 2010. **26**(4): p. 2650-2658.

9. Miller, R., et al., *Dilational and shear rheology of adsorption layers at liquid interfaces.* Colloids and Surfaces a-Physicochemical and Engineering Aspects, 1996. **111**(1-2): p. 75-118.

10. Smith, R.D. and J.C. Berg, *The collapse of surfactant monolayers at the airâ€"water interface.* Journal of Colloid and Interface Science, 1980. **74**(1): p. 273-286.

11. Kato, T., Y. Hirobe, and M. Kato, *the time of observation of pi-a isotherms .2. A possibility that so-called solid films in pi-a isotherms of monolayers of long-chain acids may not correspond to the 2-dimensional solids but to the 1st-order phase-transition regions from 2-dimensional liquids to solids.* Langmuir, 1991. **7**(10): p. 2208-2212.

12. Lee, K.Y.C., *Collapse Mechanisms of Langmuir Monolayers.* Annual Review of Physical Chemistry, 2000. **59**: p. 771-791.

13. Lee, Y.L. and K.L. Liu, *Relaxation behaviors of monolayers of octadecylamine and stearic acid at the air/water interface.* Langmuir, 2004. **20**(8): p. 3180-3187.

14. Vollhardt, D. and U. Retter, *Growth of preformed 3D nuclei in Langmuir monolayers below critical supersaturation.* Langmuir, 1998. **14**(25): p. 7250-7254.

15. Patil G.S., Matthews R. H., and Cornwell D.G., *Kinetics of the Process of Desorption From Fatty Acid Monolayers.* Journal of Lipid Research, 1973. **14**: p. 26-31.

16. Gilman, J.B., et al., *Selectivity and stability of organic films at the air-aqueous interface.* Journal of Colloid and Interface Science, 2004. **280**(1): p. 234-243.

17. Brooks, J.H. and A.E. Alexander, in *Retardation of Evaporation by Monolayers*, V.K. La Mer, Editor. 1962, Academic Press: Naw York. p. 245.

18. Xu, S., K. Miyano, and B.M. Abraham, *The Effect pf pH on Monolayer Stability.* Journal of Colloid and Interface Science, 1982. **89**(2): p. 581-583.

19. Carry, A. and E.K. Rideal, *The Behaviour of Crystals and Lenses of fats on the Surface of Water. Part II. The Effect of Temperature on Equilibrium Pressure.* Proceedings of the Royal Society, 1925. **A109**: p. 318-330.

20. Vollhardt, D., U. Retter, and S. Siegel, *Nucleation in insoluble monolayers II: Constant pressure relaxation of octodecanoic acid monolayers.* Thin Solid Films, 1991. **199**(1): p. 189-199.

21. Vollhardt, D., *Nucleation in monolayers.* Advances in Colloid and Interface Science, 2006. **123**: p. 173-188.

22. Patil, G.S., R.H. Matthews, and D.G. Cornwell, *Estimation of surface area and counterion binding characteristics in fatty amine monolayers from desorption kinetics.* Journal of Lipid Research, 1976. **17**(3): p. 197-202.

23. Matuura, R., K. Sekita, and K. Motomura, *The Desorption of Monolayers of Fatty Acids*, in *Chimie, Physique et Applications Pratiques des Agents de Surface*. 1969, Ediciones Unidas: Barcelona. p. 375-381.

24. Ter Minassian-Saraga, L., *Etudes de l'adsorption et de la desorption aux surfaces liquides.* Journal de Chimie Physique, 1955. **52**: p. 181-200.

25. Ter Minassian-Saraga, L., *Recent Work on Spread Monolayers, Adsorption and Desorption.* Journal of Colloid Science, 1956. **11**: p. 398-418.

26. Johann, R. and D. Vollhardt, *Texture features of long-chain fatty acid monolayers at high pH of the aqueous subphase.* Materials Science and Engineering: C, 1999. **8-9**: p. 35-42.

27. Aveyard, R., et al., *stability of insoluble monolayers and ionization of langmuir-blodgett multilayers of octadecanoic acid.* Thin Solid Films, 1990. **188**(2): p. 361-373.

28. Kanicky, J.R. and D.O. Shah, *Effect of Degree, Type, and Position of Unsaturation on the pKa of Long-Chain Fatty Acids.* Journal of Colloid and Interface Science, 2002. **256**: p. 201-207.

29. Brandal, Ø. and J. Sjöblom, *Interfacial Behavior of Naphthenic Acids and Multivalent Cations in Systems with Oil and Water. II: Formation and Stability of Metal Naphthenate Films at Oil-Water Interfaces.* Journal of Dispersion Science and Technology, 2005. **26**(1): p. 53 - 58.

30. de Ruiter, R., et al., *Influence of Cationic Composition and pH on the Formation of Metal Stearates at Oil-Water Interfaces.* Langmuir, 2011. **27**: p. 8738-8747.

31. Tang, C.Y., Z.S. Huang, and H.C. Allen, *Interfacial Water Structure and Effects of Mg(2+) and Ca(2+) Binding to the COOH Headgroup of a Palmitic Acid Monolayer Studied by Sum Frequency Spectroscopy.* Journal of Physical Chemistry B, 2011. **115**(1): p. 34-40.

32. Tang, C.Y., Z.S.A. Huang, and H.C. Allen, *Binding of Mg(2+) and Ca(2+) to Palmitic Acid and Deprotonation of the COOH Headgroup Studied by Vibrational Sum Frequency Generation Spectroscopy.* Journal of Physical Chemistry B, 2010. **114**(51): p. 17068-17076.

33. Kundu, S., A. Datta, and S. Hazra, *Effect of Metal Ions on Monolayer Collapses.* Langmuir, 2005. **21**: p. 5894-5900.

34. Kundu, S. and D. Langevin, *Fatty acid monolayer dissociation and collapse: Effect of pH and cations.* Colloids and Surfaces a-Physicochemical and Engineering Aspects, 2008. **325**(1-2): p. 81-85.

35. McFate, C., D. Ward, and J. Olmsted, *Organized Collapse of Fatty-Acid Monolayers.* Langmuir, 1993. **9**(4): p. 1036-1039.

36. Shih, M.C., et al., *Pressure and pH Dependence of the Structure of a Fatty Acid Monolayer With Calcium Ions in the Subphase.* Journal of Chemical Physics, 1992. **2**: p. 1556-1559.

37. Neuman, R.D., *Stearic Acid and Calcium Stearate Monolayer Collapse.* Journal of Colloid and Interface Science, 1976. **56**(3): p. 505-510.

38. Rabinovitch, W., R.F. Robertson, and S.G. Mason, *Relaxation of Surface Pressure and Collapse of Unimolecular Films of Stearic Acid.* Canadian Journal of Chemistry, 1960. **38**: p. 1881-1890.

39. Shaitan, K.V. and P. Pustoshilov, *Molecular Dynamics of Stearic Acid Monolayer.* Molecular Biophysics, 1999. **44**(3): p. 429-434.

40. Smith, R.D. and J.C. Berg, *Collapse of Surfactant Monolayers at the Air-Water Interface.* Journal of Colloid and Interface Science, 1980. **74**(1): p. 273-286.

41. Badre, C., et al., *Effects of nanorod structure and conformation of fatty acid self-assembled layers on superhydrophobicity of zinc oxide surface.* Journal of Colloid and Interface Science, 2007. **316**(2): p. 233-237.

42. Darrow, D.C., *body-fluid physiology - the relation of tissue composition to problems of water and electrolyte balance.* New England Journal of Medicine, 1945. **233**(4): p. 91-97.

43. Boldt, J., *Saline versus balanced hydroxyethyl starch: does it matter?* Current Opinion in Anesthesiology, 2008. **21**(5): p. 679-683.

44. Lager, A., K.J. Webb, and I.R. Collins. *LoSal Enhanced Oil Recovery: Evidence of Enhanced Oil Recovery at the Reservoir Scale*. in *SPE/DOE Symposium on Improved Oil Recovery*. 2008. Tulsa, Oklahoma, USA: Society of Petroleum Engineers.

45. Kester, D.R., et al., *Preparation of Artificial Sea Water.* Limnology and Oceanography, 1967. **12**(1): p. 176-179.

46. Azzam R.M.A. and Bashara N.M., *Ellipsometry and Polarized Light*. 1977, Amsterdam – New York – Oxford: North-Holland Publishing Company.

47. Tompkins H.G. and Irene E.A., *Handbook of Ellipsometry*. 2005: Springer.

48. Overbeck, G.A. and D. Mobius, *a new phase in the generalized phase-diagram of monolayer films of long-chain fatty-acids.* Journal of Physical Chemistry, 1993. **97**(30): p. 7999-8004.

49. Bibo, A.M. and I.R. Peterson, *phase-diagrams of monolayers of the long-chain fatty-acids.* Advanced Materials, 1990. **2**(6-7): p. 309-311.

50. Riviere, S., et al., *Textures and phase transitions in Langmuir monolayers of fatty acids. A comparative Brewster angle microscope and polarized fluorescence microscope study.* The Journal of Chemical Physics, 1994. **101**(11): p. 10045-10051.

51. William B. Russel, W.B.R., D. A. Saville, William Raymond Schowalter, *Colloidal dispersions*. 1989: Cambridge University Press. 525.

52. Schwartz, D.K., et al., *surface order and stability of langmuir-blodgett-films.* Science, 1992. **257**(5069): p. 508-511.

53. Sears, D.F. and J.H. Schulman, *Influence of Water Structures on the Surface Pressure, Surface Potential, and Area of Soap Monolayers of Lithium, Sodium, Potassium, and Calcium.* The Journal of Physical Chemistry, 1964. **68**(12): p. 3529-3534.

54. Lee, K.Y.C., *Collapse mechanisms of Langmuir monolayers.* Annual Review of Physical Chemistry, 2008. **59**: p. 771-791.

55. Cerro, R.L., *Moving contact lines and Langmuir-Blodgett film deposition.* Journal of Colloid and Interface Science, 2003. **257**(2): p. 276-283.

56. Dekeyser, P. and P. Joos, *kinetics of monolayer collapse as a nucleation process.* Journal of Physical Chemistry, 1984. **88**(2): p. 274-280.

57. Vollhardt, D. and U. Retter, *Nucleation in insoluble monolayers. 1. Nucleation and growth model for relaxation of metastable monolayers.* The Journal of Physical Chemistry, 1991. **95**(9): p. 3723-3727.

58. Ghaicha, L., A.K. Chattopadhyay, and H.A. Tajmirriahi, *Behavior of Stearic Acid Monolayers in Presence of Concentrated Ammonium Nitrate Solution Substrate.* Langmuir, 1991. **7**(10): p. 2007-2009.

Appendix

595 ***Table A1.*** *Results of fitting the Vollhardt model to the relaxation data of SA films on ASW of varying total salt concentration and pH 3: x – characteristic quantity determining particular nucleation mechanism, K_x –transformation constant , t_i – induction time, R^2 – correlation coefficient. We consider first 20 min of the relaxation process.*

	Pressure [mN/m]	Sub-phase	x	K_x	t_i [s]	R^2
pH 3	30	Water	3.36	1.39×10^{-11}	-120.82	0.9985
		1% ASW	2.91	2.53×10^{-10}	-180.77	0.9923
		10% ASW	3.25	2.52×10^{-11}	-216.32	0.9995
		ASW	2.17	4.26×10^{-8}	-176.58	0.9895
pH 7	30	Water	3.00	1.04×10^{-10}	-214.05	0.9919
	50	1% ASW	2.30	5.57×10^{-8}	-76.63	0.9967
pH 10	30	Water	0.73	2.02×10^{-3}	-11.51	0.9974
	50	Water	0.73	4.12×10^{-3}	0	0.9684

Table A2*. Estimates of the desorption coefficients of SA molecules from films formed on sub-phase of varying total salt concentration and pH. K'_1 is defined as $d(\ln(A/A_0))/d(t^{1/2})$, and K'_2 is defined as $d(\ln(A/A_0))/d(t)$.*

	Pressure [mN/m]	Sub-phase	K'_1 [$s^{-1/2}$]	K'_2 [s^{-1}]	K'_2/K'_1	R^2 ($t^{1/2}$)	R^2 (t)
pH 3	20	10% ASW	0.0005	7.55×10^{-6}	1.51×10^{-2}	0.9803	0.9946
		100% ASW	0.0004	5.86×10^{-6}	1.47×10^{-2}	0.9822	0.9901
pH 7	30	1% ASW	0.0002	1.35×10^{-6}	6.75×10^{-3}	0.9490	0.8985
		10% ASW	0.0005	3.15×10^{-6}	6.30×10^{-3}	0.9909	0.9421
		100% ASW	0.0006	3.36×10^{-6}	5.60×10^{-3}	0.9706	0.9853
	50	10% ASW	0.0002	2.52×10^{-5}	1.26×10^{-1}	0.9410	0.9977
		100% ASW	0.0004	4.51×10^{-6}	1.13×10^{-2}	0.9079	0.9844
pH 10	30	1% ASW	0.0004	2.62×10^{-6}	6.55×10^{-3}	0.9785	0.9695
		10% ASW	0.0007	-	-	0.9963	-
		100% ASW	0.0006	3.24×10^{-6}	5.40×10^{-3}	0.9705	0.9730
	50	1% ASW	0.0008	3.90×10^{-5}	4.88×10^{-2}	0.9585	0.9992
		10% ASW	0.0007	2.39×10^{-5}	3.41×10^{-2}	0.9821	0.9993
		100% ASW	0.0008	1.04×10^{-5}	1.30×10^{-2}	0.9973	0.9956

600

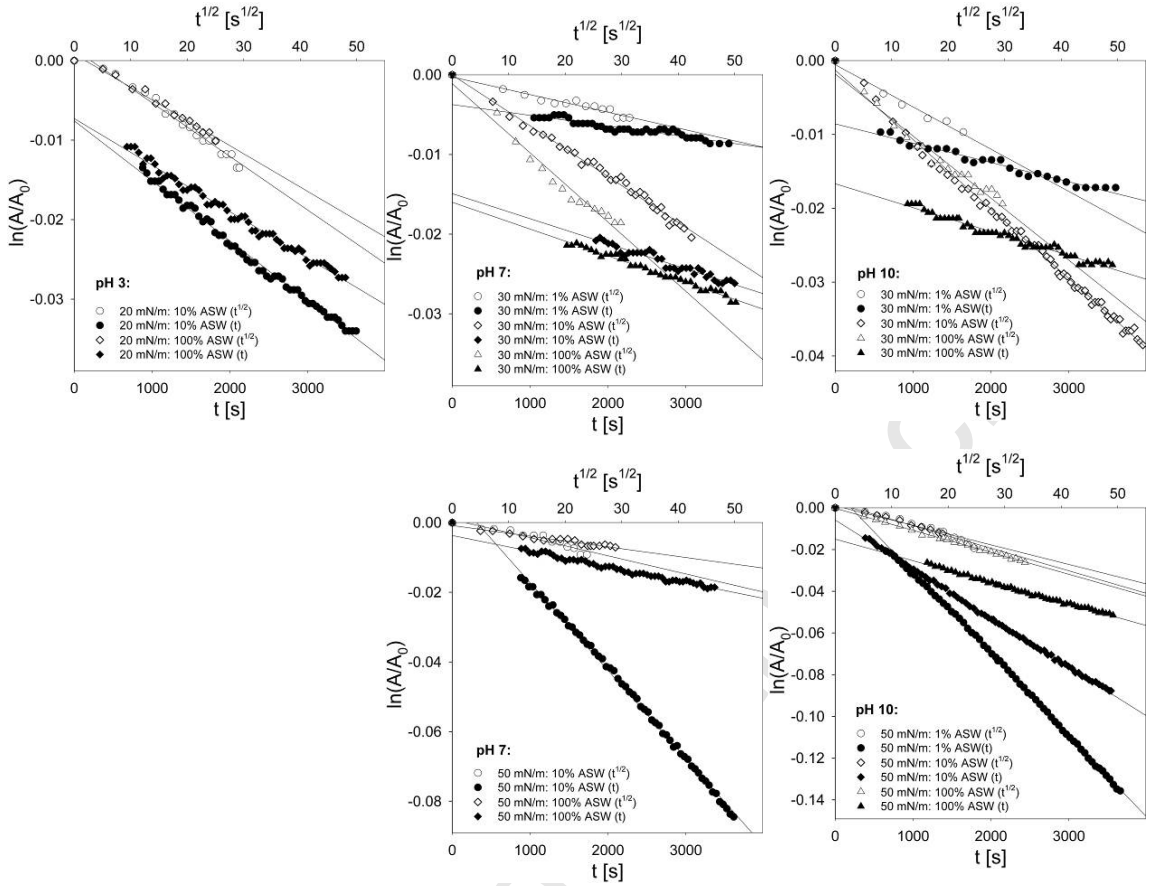

***Figure A1**. Change of surface area per molecule during relaxation of SA films at constant pressure on sub-phases of varying total salt concentration and pH. $ln(A/A_0)$ is plotted as a function of t (solid symbols, lower scale) and $t^{1/2}$ (open symbols, upper scale). Solid lines represent linear fits to the experimental data and are extended to the axis for clarity.*

605

Graphical Abstract

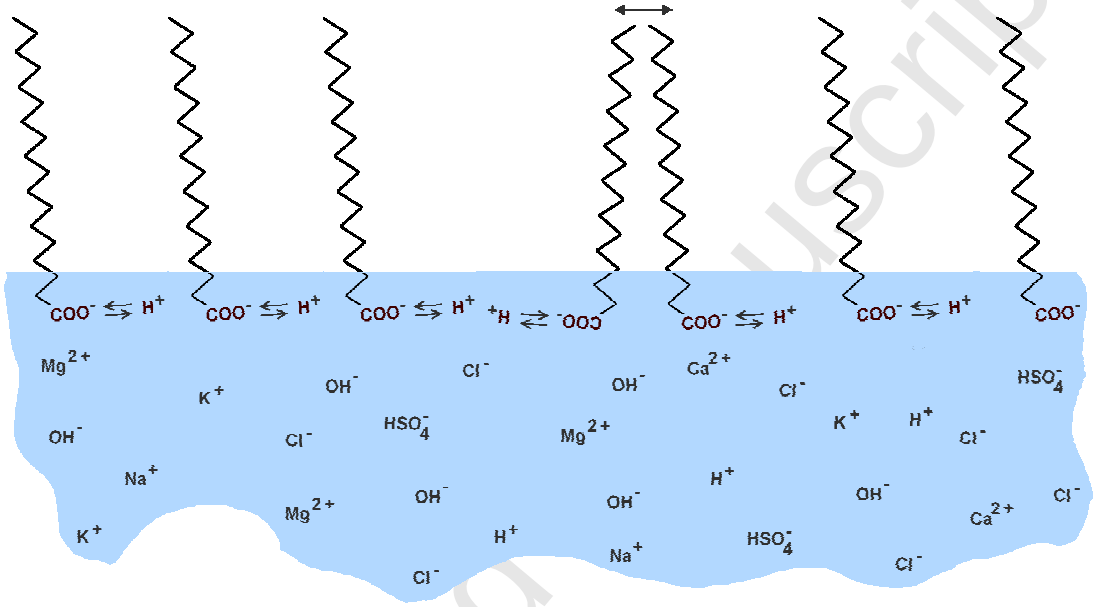

610

Highlights

- Langmuir films of stearic acid can be stabilized by increasing salt concentration and/or pH of the sub-phase.
- 3D solid phase is formed under acidic conditions.
- Dissolution of molecules into sub-phase occurs only at high pH and low salt concentration.
- The influence of multicomponent salt is a combination of ionic strength and specific ion effects.